Orientation Distribution and Layerlike Morphology in Extrusion-Molded Sheets of a Liquid Crystalline Copolyester Amide

AKIRA KAITO,* MUTSUMASA KYOTANI, and KAZUO NAKAYAMA

National Institute of Materials and Chemical Research, 1-1 Higashi, Tsukuba, Ibaraki 305, Japan

SYNOPSIS

Fracture surface morphology and orientation distribution in the extrusion-molded sheets of a thermotropic liquid crystalline copolyester amide were investigated by scanning electron microscopy (SEM), wide-angle X-ray diffraction (WAXD), and polarized Fourier transform infrared (FTIR) microspectroscopy. The layerlike morphology consisting of two outer layers and a central layer between them was observed on the fracture surface. The microscopic orientation functions in the extrusion-molded sheets were evaluated from the polarized FTIR microspectra that were measured in the microscopic domain 40 μm wide using a redundantly apertured infrared microscope. The microscopic orientation function in the outer layer was shown to be higher than that in the central layer. The effects of the draw-down ratio and extrusion temperature on the orientation distribution and the layerlike morphology are discussed. © 1993 John Wiley & Sons, Inc.

INTRODUCTION

Thermotropic liquid crystalline polymers (LCP) have attracted the interests of many researchers, because they can be processed directly from the melt into high-performance materials by conventional processing techniques, such as melt spinning, extrusion molding, and injection molding. Since the molecular chains of LCP follow the flow direction of the polymer melt in the molding process, the oriented morphologies are developed in the fabrics of LCP. It is further pointed out that the complex flow in the molding process causes the structural distribution in the materials of LCP.[1,2] A skin–core structure originating from the difference in orientation was recognized by the morphological observations using scanning electron microscopy (SEM) and polarized optical microscopy.[1-5] Based on the morphological structures, the hierarchical structural model was proposed for the injection-molded parts of an LCP.[4,6] A layerlike morphology was confirmed by the observation of SEM for the extrusion-molded sheets of a thermotropic liquid crystalline copolyester.[7] The orientation distribution in the materials of LCP has been extensively investigated by wide-angle X-ray diffraction (WAXD),[1,8-10] birefringence measurements,[1,5] and polarized attenuated total reflection (ATR)/Fourier transform infrared (FTIR) spectroscopy.[11] Recently, we demonstrated that polarized FTIR microspectroscopy was a powerful technique for evaluating the molecular orientation in the microscopic domain of the polymeric materials.[12,13] Polarized FTIR microspectroscopy was applied to obtain the orientation profiles in extrusion-molded strands and sheets of thermotropic LCP.

In this work, the molecular orientation and morphological structure in extrusion-molded sheets of a liquid crystalline copolyester amide are studied with WAXD, SEM, and polarized FTIR microspectroscopy. A great deal of attention was focused on the effects of draw-down ratio and extrusion temperature on the structures of the LCP sheets. The layerlike morphology observed by SEM is discussed in relation to the orientation distribution evaluated by polarized FTIR microspectroscopy.

* To whom correspondence should be addressed.

Journal of Applied Polymer Science, Vol. 48, 2147–2159 (1993)
 CCC 0021-8995/93/122147-13

EXPERIMENTAL

Sample Preparation

The polymer studied in this work is a thermotropic liquid crystalline copolyester amide polymerized from 2-hydroxy-6-naphthoic acid, terephthalic acid, and 4-aminophenol. Synthesis and properties of the copolyester amide were reported by Calundann and Jaffe.[14] The polymer shows a crystal–mesophase transition at 282°C on a differential scanning calorimeter. Prior to the extrusion molding, pellets (Polyplastic Co.) of the polymer were dried at 90°C for 12 h and at 150°C for 3 h. Sheets of the copolyester amide were extrusion-molded using a twin-screw extruder, Labo Plastomill Model 50C150 (Toyoseiki Co.), equipped with a coat-hanger die. The extruder is composed of cylinders 20 mm in diameter and a pair of screws rotating in the opposite direction. The dimension of the die orifice is 150 mm wide, and the die gap was adjusted at 2 mm. The die temperature (T_E) was varied in the range of 290–340°C. The extruded sheets were drawn-down in the molten state by winding them using a pair of rollers whose temperature was controlled at 120°C. The extrusion molding was carried out at a constant screw speed of 20 rpm. The draw-down ratio was controlled by changing the takeup velocity in the range of 0.6–3.2 m/min.

Characterization

The dynamic storage modulus was measured at 110 Hz with a dynamic viscoelastometer, Rheovibron DDV-III-EA (Orientec Co.). The second moments of crystal orientation functions were determined from the azimuthal intensity distribution of wide-angle X-ray diffraction (WAXD). Ni-filtered CuKα radiation generated by a Geiger Flex XGC-20 (Rigaku Denki Co.) was used as an incident X-ray beam. The WAXD intensity was measured by use of a scintillation counter and a pulse height analyzer.

The fracture surface was observed with a scanning electron microscope, Akashi Model DS-130. The extrusion-molded sheets were fractured along the extrusion direction, and the surfaces were coated with gold.

The extrusion-molded sheets were microtomed to a thickness of 10 μm, after the sheets were embedded in an epoxy resin. The microtomed sections were used for the measurements of polarized FTIR microspectra. The FTIR microspectra were measured with a Perkin-Elmer Model 1800 FTIR spectrometer equipped with a liquid-nitrogen-cooled MCT detector. One thousand scans of 4 cm^{-1} resolution were averaged to achieve a sufficient signal-to-noise ratio. The microbeam radiation was obtained with a redundantly apertured infrared microscope, IR-plan Model 100 (Spectra-Tec, Inc.), which was composed of two apertures, a Cassegranian objective, and a condenser. Infrared radiation was focused on the sample by a 15× objective after passing through the first aperture, so as to form a sample image with a 40 × 200 μm dimension. The transmitted infrared beam passed through a 10× condenser and was masked again by the lower aperture to remove scattered radiations. The polarized FTIR microspectra were obtained by changing the polarization direction of a wire-grid polarizer that was placed under the condenser.

RESULTS AND DISCUSSION

Extrusion-molding Process

The draw-down ratio (λ) is shown as a function of takeup speed in Figure 1. The draw-down ratio increases with increasing takeup speed, but the relation between draw-down ratio and takeup speed deviates from linear function. As molten polymers behave as viscoelastic materials, tensile stress acts on the molten polymers in the die. At higher takeup velocity, the tensile stress increases and accelerates the polymer flow in the die. As a result, mass output increases with increasing takeup velocity. The measured value of mass output is about 29–36 g/min at a takeup velocity of 0.6 m/min and amounts to 35–45 g/min at higher takeup velocities.

At the same takeup velocity, mass output increases and the draw-down ratio decreases with the rise in the die temperature. The effects of the die temperature on the draw-down ratio might be originated in the change in the viscosity of the polymer.

Mechanical Properties

The dynamic storage modulus at 25°C is shown in Figure 2. The dynamic storage modulus increases with increasing draw-down ratio at lower values ($\lambda < 15$), but the effect of the draw-down on the dynamic storage modulus saturates at a higher draw-down ratio. At a lower draw-down ratio, the dynamic storage modulus increases with the rise in the extrusion temperature.

The mechanical properties of melt-spun LCP fibers have been extensively studied as a function of the draw-down ratio.[15–17] It was found that the me-

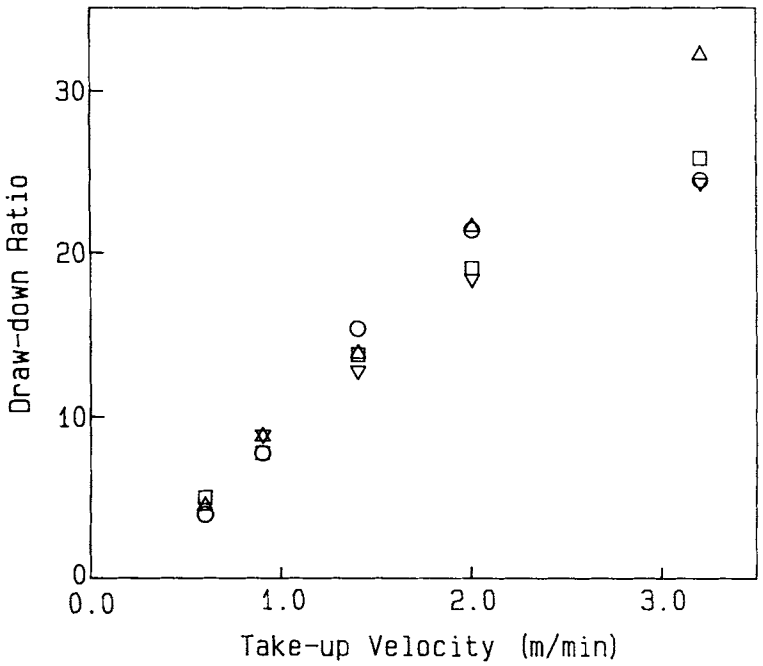

Figure 1 Relation between draw-down ratio and takeup velocity: (△) T_E = 290°C; (○) T_E = 300°C; (□) T_E = 320°C; (▽) T_E = 340°C.

chanical properties of LCP fibers were improved with increasing draw-down ratios and that the increase of the mechanical properties became gradual at higher draw-down ratios. The effects of the draw-down process on the LCP fibers are similar to those on the LCP sheets.

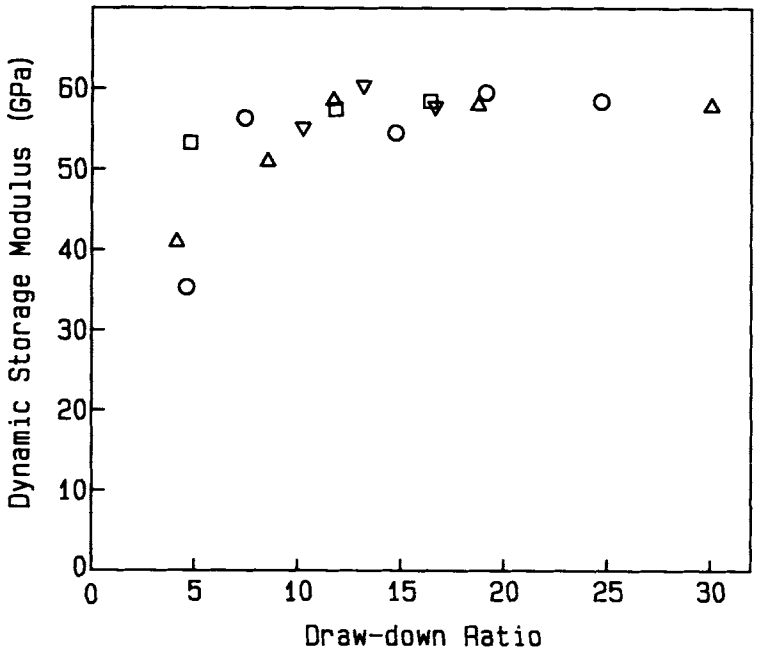

Figure 2 Dynamic storage modulus at 25°C and 110 Hz as a function of draw-down ratio: (△) T_E = 290°C; (○) T_E = 300°C; (□) T_E = 320°C; (▽) T_E = 340°C.

Crystal Orientation Function

The second moment of orientation distribution function of the LCP sheets was obtained from the azimuthal intensity distribution of the meridional WAXD reflection observed at $2\theta = 43.0°$. The dependence of orientation functions on the draw-down ratio is shown in Figure 3. The WAXD reflection originates from the 004 plane of the naphthoic acid units and the 003 plane of the *para*-substituted benzene units. The orientation distribution is formed inside the extrusion-molded LCP sheets, and the orientation function obtained from the WAXD corresponds to the crystal orientation function averaged over the sample. The crystal orientation functions depend not only on the draw-down ratio, but also on the extrusion temperature (T_E). If the extrusion temperature is lower (T_E = 290 or 300°C), the orientation function increases with increasing draw-down ratios at lower values ($\lambda < 15$) and approaches a constant value at higher draw-down ratios. At T_E = 320 and 340°C, the values of the orientation functions are constant in the draw-down range of $7 < \lambda < 20$. At a lower draw-down ratio ($\lambda < 15$), the orientation function increases with the rise in extrusion temperature from 300 to 320°C. The dependence of the mechanical properties on the draw-down ratio is closely correlated with the changes in molecular orientation.

Fracture Surface Morphology

Fracture surface morphologies of extrusion-molded sheets are shown in Figure 4. The sheets were fractured parallel to the extrusion direction (ED) and normal to the sheet plane. The sheets extruded at T_E = 290°C are shown to be composed of three macrolayers [Fig. 4(a) and (b)]. The thickness of each layer is approximately one-third of the entire sheet thickness. The boundaries between the central and outer layers are more obvious in the sheet with a lower draw-down ratio. Cracks are generated in the boundary of the macrolayers of the sheet of $\lambda = 3.97$ [Fig. 4(a)]. The sheets tend to cleave parallel to the sheet plane, giving rise to flakelike fibrils on the fracture surface.

The boundaries between the central and outer layers become obscure with the rise in extrusion temperature from T_E = 290°C to T_E = 320°C [Fig. 4(c) and (d)]. The layerlike structure still exists at a lower draw-down ratio [Fig. 4(c)], whereas a uniform structure is formed across the thickness direction in the sheet with a higher draw-down ratio [Fig. 4(d)]. At a higher draw-down ratio, thin fibrils are highly oriented in the extrusion direction.

Magnified views of the SEM photograph in Figure 4(a) are given in Figure 5. In the outer layer of the sheet, thin fibrils 0.2–0.5 μm in diameter densely pack the layer and are highly oriented parallel to the extrusion direction [Fig. 5(a)]. Fibrils in the

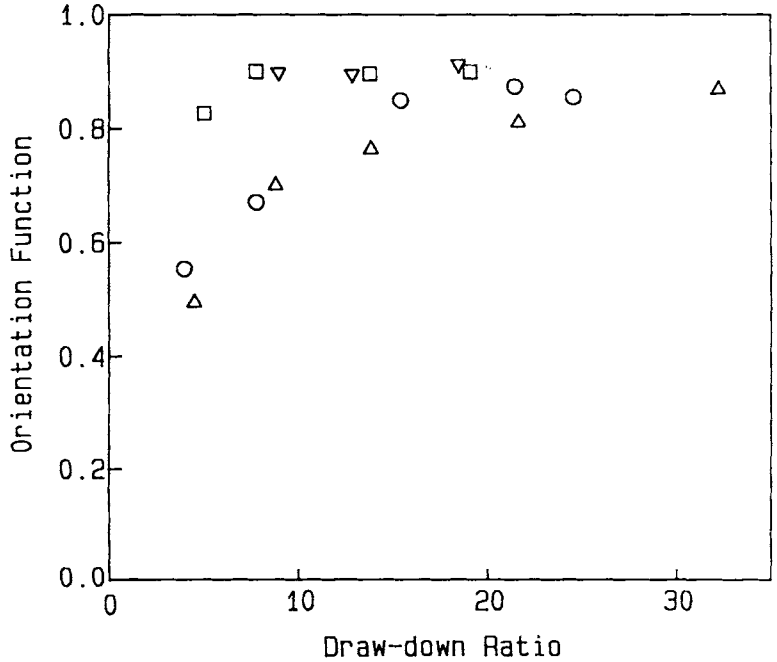

Figure 3 Crystal orientation functions obtained from WAXD as a function of draw-down ratio: (△) T_E = 290°C; (○) T_E = 300°C; (□) T_E = 320°C; (▽) T_E = 340°C.

central layer are thicker than those in the outer layer and the fibrous morphology is not fully developed in the central layer [Fig. 5(b)].

Magnified views of the SEM photograph in Figure 4(c) are given in Figure 6. The fibrous structure is well developed both in the outer and central layers of the sheet (T_E = 320°C, λ = 4.76). Thin fibrils 0.2–1 μm in diameter are highly oriented in the extrusion direction in the outer layer [Fig. 6(a)]. Fibrils in the central layer are thicker and are less oriented than those in the outer layer.

The sheets were fractured parallel to the sheet plane and were delaminated into the three macrolayers. The interface between the outer and central layers was observed with SEM. The morphologies of the surface of the delaminated macrolayers are shown in Figure 7. A number of flakelike fibrils 5–10 μm wide are observed on the interface in the sheet extruded at 290°C [Fig. 7(a)]. The structure of the surface is relatively flat, because the connection of the macrolayers is loose in the sheet extruded at 290°C. On the interface of macrolayers in the sheet extruded at 320°C, however, one observes many terminals of thin fibrils that might be broken down by the delamination [Fig. 7(b)]. The roughness of the fracture surface suggests that the outer and central layers are tightly bound by a number of fibrils in the sheet extruded at 320°C.

Orientation Distribution

The polarized FTIR microspectra of a microtomed section of the LCP sheet (T_E = 290°C, λ = 4.80) are shown in Figure 8. The solid line represents the spectrum measured with polarization parallel to the extrusion direction, and the chain line is the spectrum polarized in the normal direction. The FTIR microspectra in the surface region are shown in Figure 8(a), and those in the central region are presented in Figure 8(b). The absorption band observed at 1743 cm^{-1} is assigned to the stretching of the carbonyl bond in the ester linkage, whereas the bands at 1674 and 1525 cm^{-1} are ascribed to the amide I and amide II bands, respectively. The remaining bands observed in this region are assigned to the CC stretching vibrations of the naphthalene and benzene rings. The 1606 and 1510 cm^{-1} bands originate from the benzene ring, and the 1632 and 1473 cm^{-1} bands are attributed to the naphthalene ring. The dichroic ratios in the spectra of the surface region are shown to be higher than those in the central region.

The orientation profiles were obtained by plotting the dichroic ratio of the 1473 cm^{-1} band against the ratio of distance from the center, Z, to the sheet thickness, T. If the LCP sheet is microtomed parallel to the extrusion direction and perpendicular to the sheet plane, one can measure the ratio of absorption intensity in the extrusion direction (X axis) and that in the normal direction (Z axis): A_x/A_z. On the other hand, the dichroic ratio, A_x/A_y, is obtained from the specimen microtomed parallel to the sheet plane. The orientation profile of the LCP sheet (T_E = 290°C, λ = 4.80) is shown in Figure 9. The open circles represent the dichroic ratio, A_x/A_z, and the filled circles are A_x/A_y. The mode of molecular orientation deviates from the uniaxial orientation. The dichroic ratio A_x/A_z is higher than the ratio A_x/A_y in the central region, whereas the value of A_x/A_y exceeds A_x/A_z near the surface. The orientation profiles are closely related to the fracture surface morphology. In the central layer of the fracture surface ($-0.33 < Z/T < 0.33$), the dichroic ratio remains in the range of 1.4–3.5, whereas the dichroic ratio in the outer layer is higher than 3.5. The dichroic ratio increases from the center toward the surface, and the increase of dichroic ratio is marked near the boundary of the central and outer layers.

The orientation profiles, A_x/A_z, of the LCP sheets (T_E = 320°C, λ = 4.8–24.7) are shown in Figure 10. In every sample, the dichroic ratio increases from the center toward the surface. The dichroic ratio at each position increases gradually with increasing draw-down ratio. It is found by comparing Figure 9 with Figure 10 that the microscopic orientation function increases with the rise in extrusion temperature at the similar draw-down ratio (λ = 4.8) and that the increase of orientation function with T_E is marked in the central region. The result parallels the dependence of the crystal orientation functions on the extrusion temperature.

Comparison of Orientation Function Determined by Polarized FTIR Microspectroscopy with Crystal Orientation Function Obtained by WAXD

The second moment of orientation function, f_i, is calculated from the dichroic ratio, D_i, of absorption band, i:

$$f_i = (D_i - 1)/(D_i + 2) \quad (1)$$

The orientation function f_i represents the orientation function of the transition moment of the band, i. The orientation function, f, of the polymer chain axis is calculated from the orientation function, f_i, if the angle, ω_i, between the polymer chain axis and the transition moment direction is known:

$$f = 2f_i/(3\cos^2\omega_i - 1) \quad (2)$$

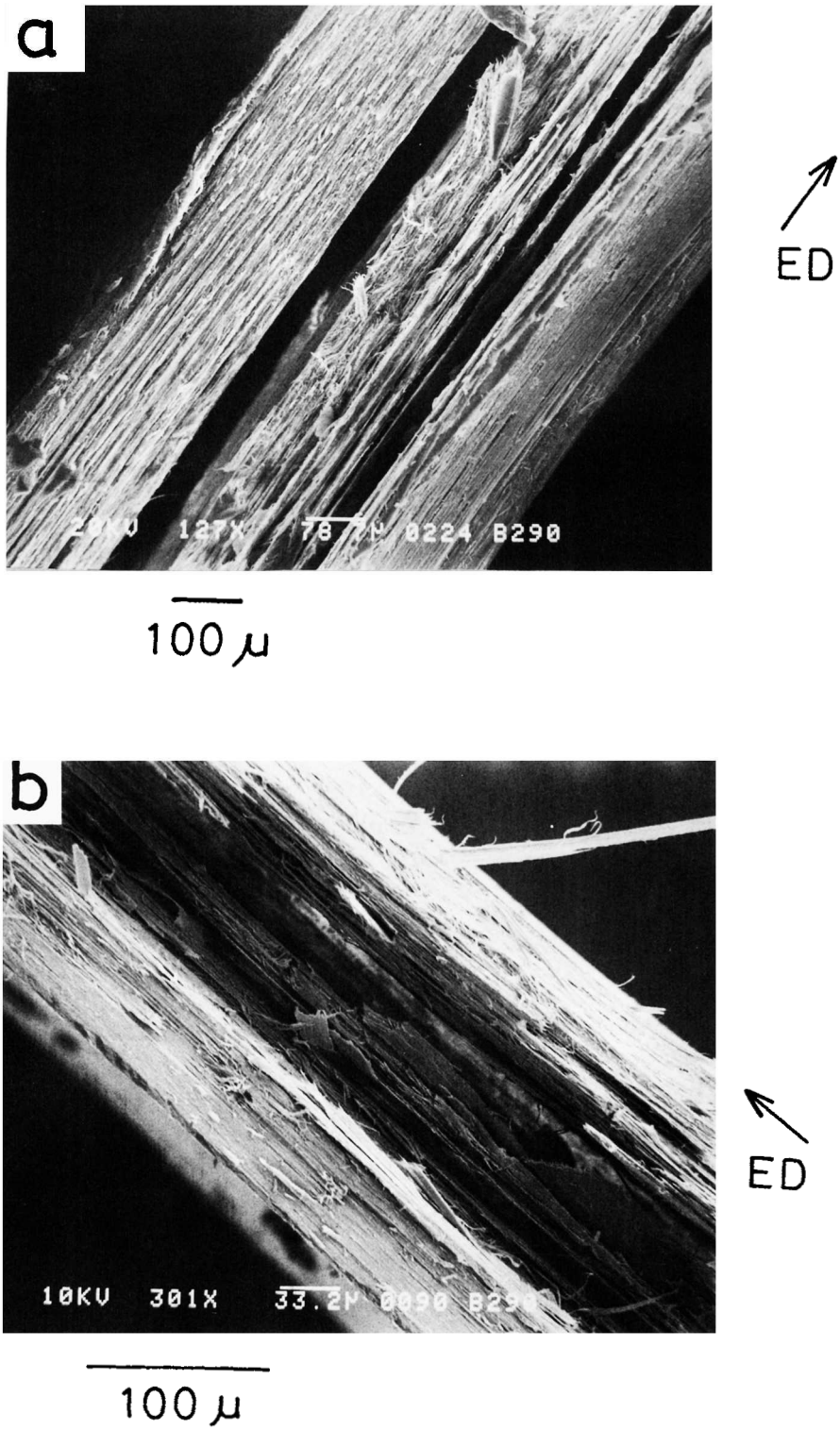

Figure 4 Fracture surface morphologies of extrusion-molded LCP sheets: (a) T_E = 290°C, λ = 3.97; (b) T_E = 290°C, λ = 11.2; (c) T_E = 320°C, λ = 4.76; (d) T_E = 340°C, λ = 11.2.

Recently, we measured the polarized ATR spectra of the liquid crystalline polyester amide.[18] The value of f_i for the 1473 cm^{-1} band in the polarized ATR spectra reaches 0.85 at a higher draw-down ratio, which provides the higher limits of the transition moment angle, ω_i. Even if the polymer chains are

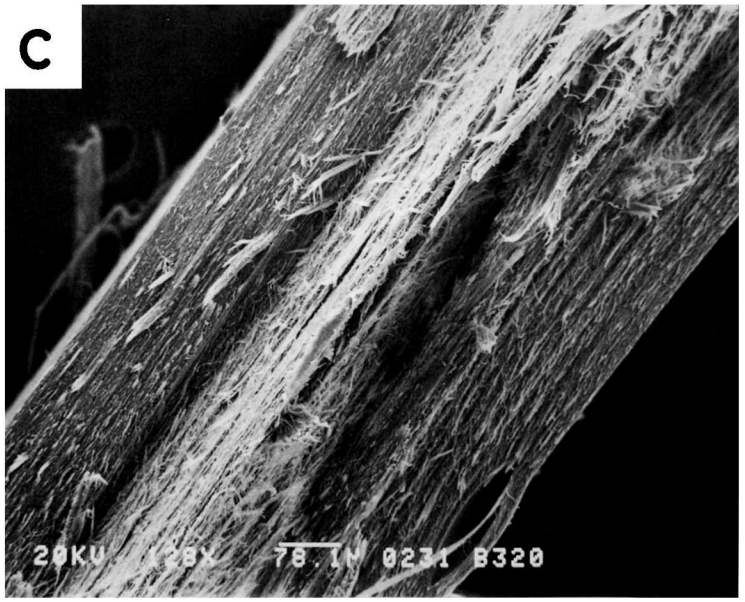

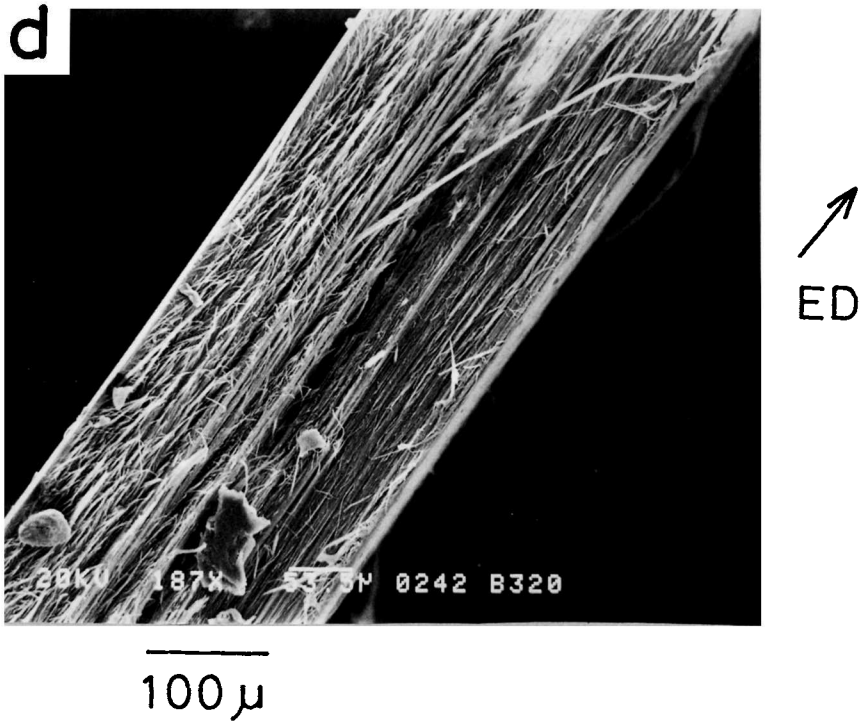

Figure 4 *(Continued from the previous page)*

completely oriented in the extrusion direction of the sample, the transition moment angle is as small as 18.4°. Thus, the value of ω_i for the 1473 cm^{-1} band lies in the range of 0–18.4°.

The bulk orientation function can be calculated by averaging the microscopic orientation function over space:

$$f(\text{bulk}) = \int_{-T/2}^{T/2} f(Z)\, dZ/T \qquad (3)$$

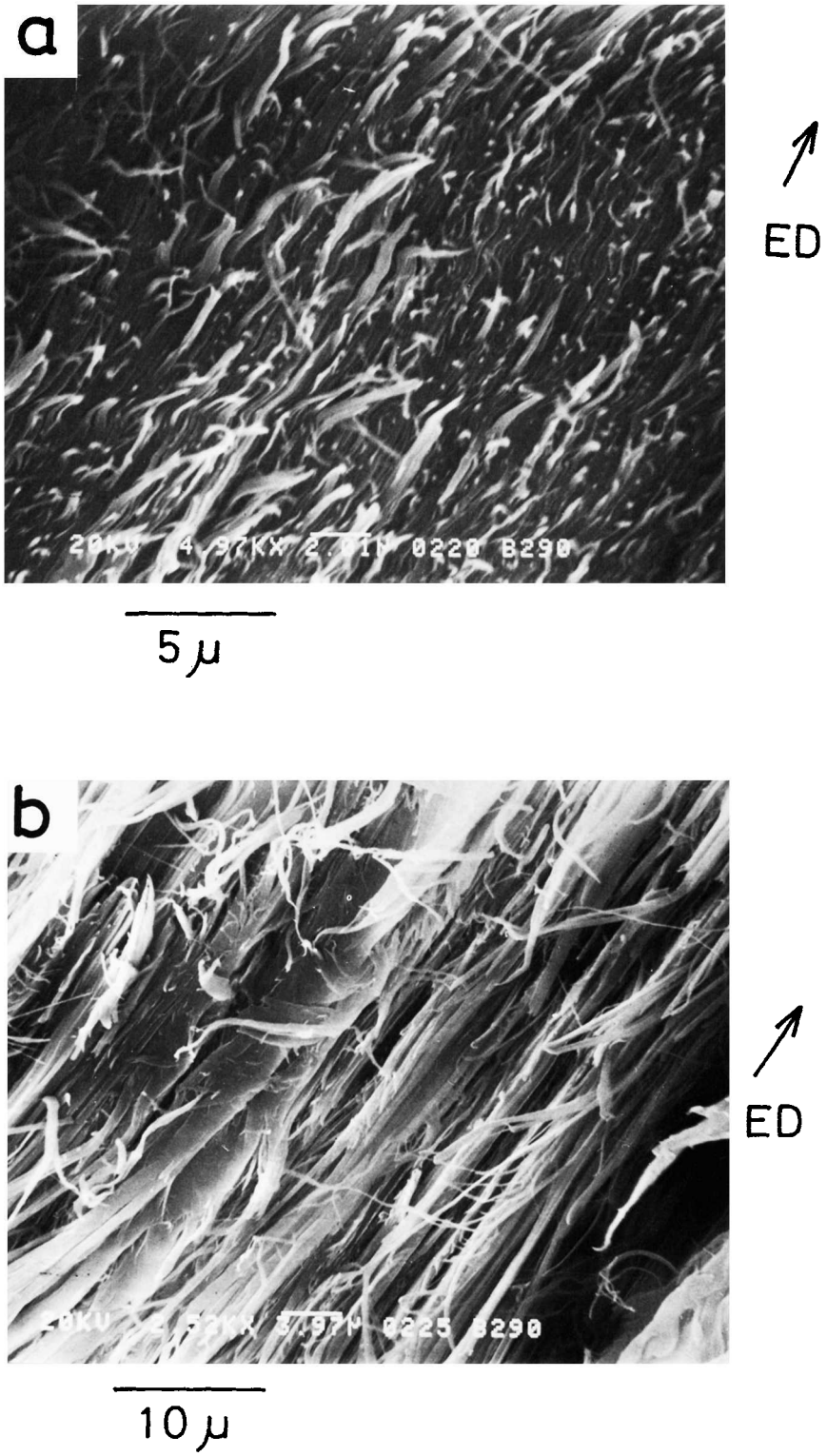

Figure 5 Fracture surface morphology of LCP sheet (T_E = 290°C, λ = 3.97): (a) outer layer; (b) central layer.

where $f(Z)$ is the microscopic orientation function at distance Z from the center of the sheet and T is the sheet thickness. The possible range of bulk orientation function, f(bulk), is calculated from microscopic orientation functions using eqs. (2) and (3), and the result is shown in Figure 11. The bulk

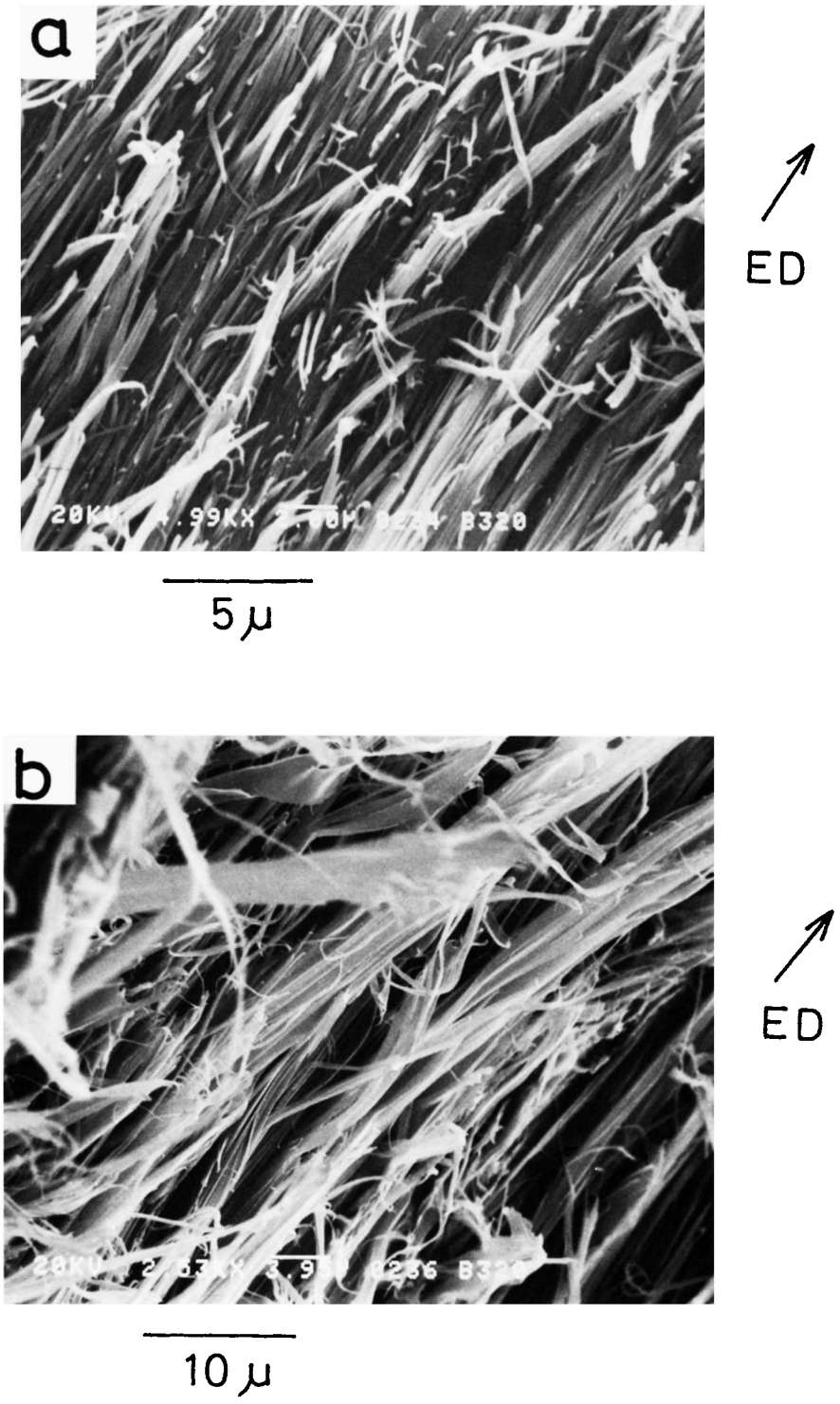

Figure 6 Fracture surface morphology of LCP sheet (T_E = 320°C, λ = 4.76): (a) outer layer; (b) central layer.

orientation function gradually increases with increasing draw-down ratio at $\lambda < 15$.

The orientation function obtained from polarized FTIR spectra tends to be lower than the orientation function determined by WAXD. The orientation function obtained from WAXD represents the bulk orientation function in the crystalline region, whereas there is contribution to the absorption band

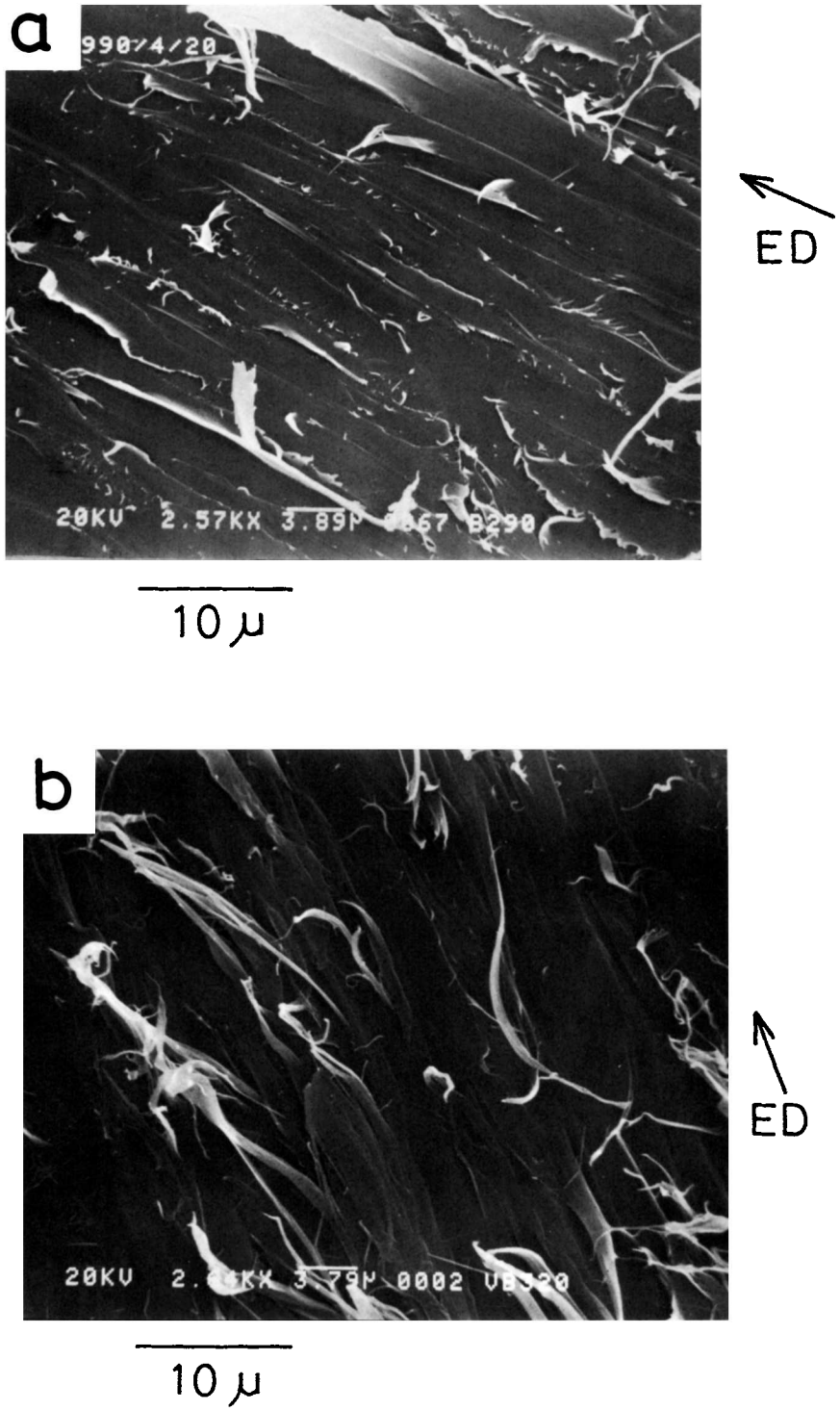

Figure 7 Morphologies of interface between outer and central layers: (a) T_E = 290°C, λ = 3.97; (b) T_E = 320°C, λ = 4.76.

from both crystalline and noncrystalline regions. The molecular chains in the crystalline region are shown to be more highly oriented to the extrusion direction than are those in the noncrystalline region.

Mechanism for the Structure Development

The orientation distribution in the extrusion-molded LCP sheets is closely related to the flow character-

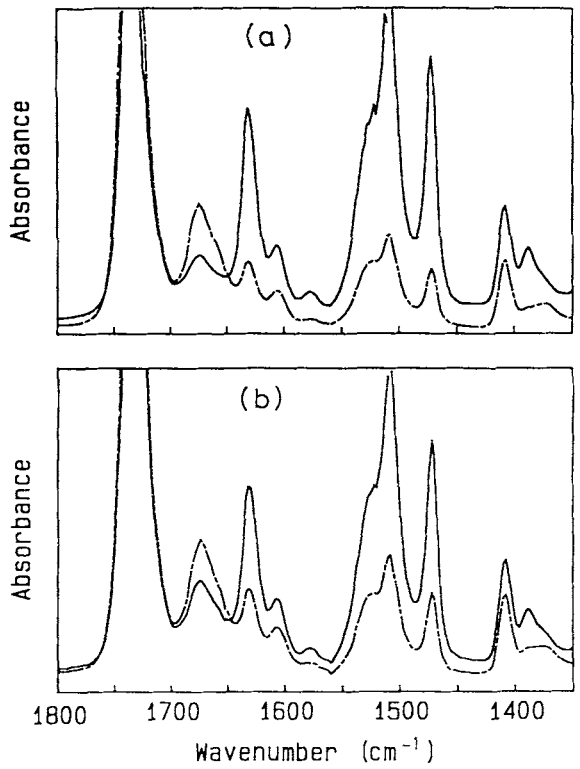

Figure 8 Polarized FTIR microspectra of a microtomed section of LCP sheet (T_E = 290°C, λ = 4.80): (a) surface region; (b) central region: (——) parallel polarization; (- - -) perpendicular polarization.

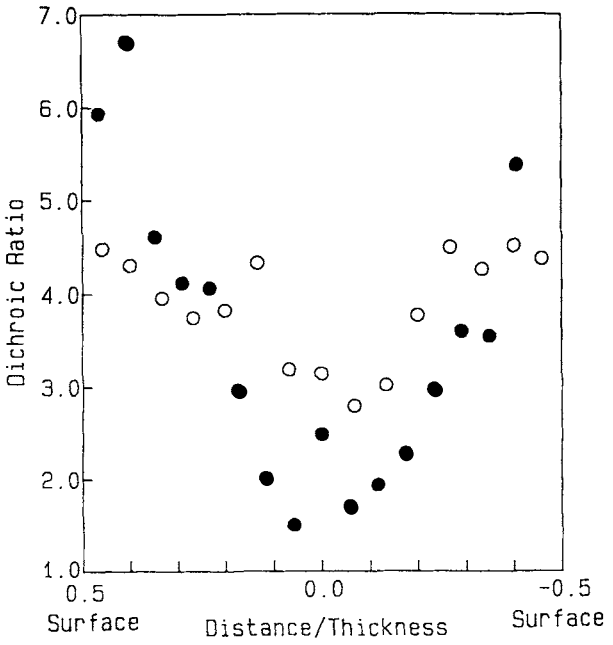

Figure 9 Orientation profile of LCP sheet (T_E = 290°C, λ = 4.80): (○) A_x/A_z; (●) A_x/A_y.

istics in the polymer melt. The semirigid molecular chains of the LCP orient in the extrusion direction by the shear flow inside the slit die and the elongational flow in the postdrawing process. The shear flow acts on orienting the polymer chains in the surface region, because the gradient of the flow velocity is higher near the die wall than at the center.[1,2] On the other hand, it was reported that the elongational flow was more effective on orienting the polymer chains than on the shear flow.[2] Inside the die, the velocity of the flow is fast at the center, but is slow near the die wall. After the polymer is extruded from the die, the velocity profile becomes constant along the thickness direction and the polymer melts are solidified. This means that the fluid elements near the surface are stretched to a higher elongation than those in the central region. Thus, the orientation distribution inside the extruded sheets can be explained by the flow behavior of the polymer melts. With increasing draw-down ratio, the fluid elements in the central region are also stretched to a high draw ratio, resulting in the high degree of orientation even in the central region.

The layerlike morphology observed on the fracture surface seems to be related to the orientation distribution. At lower extrusion temperature and lower draw-down ratio, the dichroic ratio in the surface region is much higher than that in the central

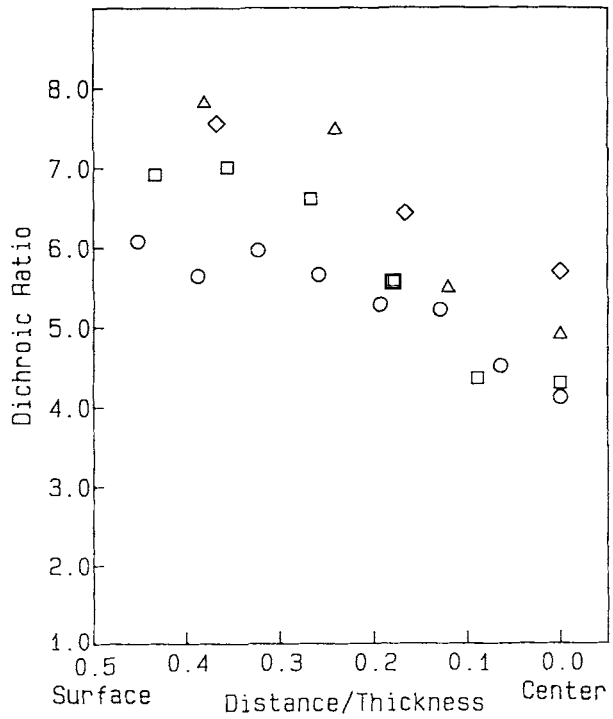

Figure 10 Orientation profiles of LCP sheets (T_E = 320°C): (○) λ = 4.88; (□) λ = 7.60; (△) λ = 14.1; (◇) λ = 24.7: the values of A_x/A_z are shown here.

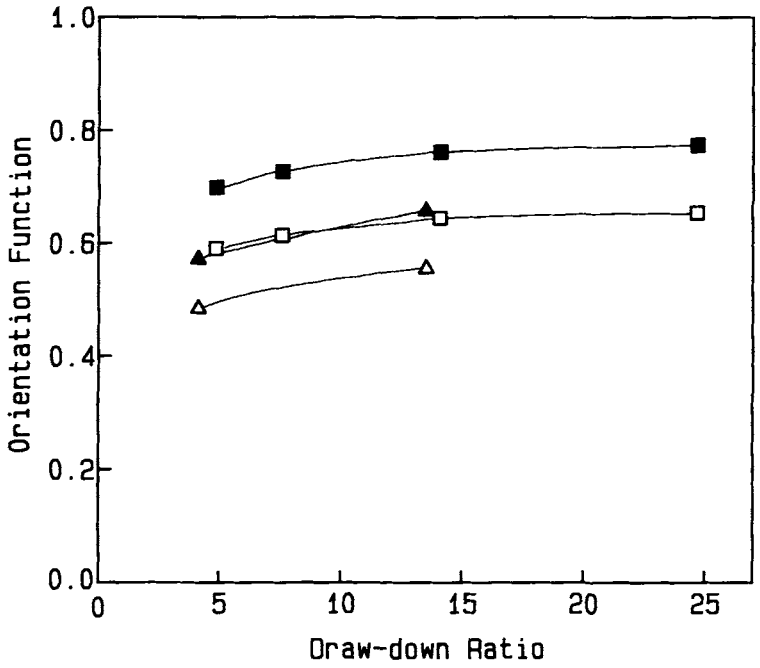

Figure 11 Possible range of bulk orientation functions obtained from the polarized FTIR microspectroscopy: (△, ▲) T_E = 290°C; (○, ●) T_E = 320°C; (△, ○) lower limit of orientation functions; (▲, ●) higher limit of orientation functions.

region, and cracks are observed at the boundary between the outer and central layers of the fracture surface. As the draw-down ratio increases and extrusion temperature rises, the variation of the microscopic orientation function with the position becomes gradual and the boundary between the outer and central layers is obscured. It is reasonable to consider that the layerlike morphology reflects the difference in molecular orientation between the outer layer and the central layer.

Takeuchi et al. reported that the thermal expansion coefficient of an LCP was dependent upon the degree of molecular orientation.[5] Based on the orientation distribution, they explained the mechanism of the band-pattern development in the shear-oriented rods of the LCP. Although the detailed mechanism for the structure development in the sheets is not clearly known, one possible explanation is that the layerlike structure is developed in the cooling process by the difference in the contraction ratio between the outer and central layers.

CONCLUSIONS

Oriented structure is developed in extrusion-molded sheets of a liquid crystalline copolyester amide. The mechanical property and the orientation function were investigated as a function of draw-down ratio and extrusion temperature. The dynamic storage modulus and the crystal orientation function increase with increasing draw-down ratio, and the effects of the draw-down process tend to saturate at a higher draw-down ratio.

The layerlike morphology consisting of two outer layers and a central layer between them is observed on the SEM photograph of the fracture surface. The boundary of the outer and central layers obvious in the sheet with low draw-down ratio (λ = 3.97) extruded at low temperature (T_E = 290°C). The marked difference is observed in the molecular orientation between the outer and central layers of the LCP sheet (T_E = 290°C, λ = 3.97).

The layerlike morphology is closely related to the orientation distribution inside the sample. With an increasing draw-down ratio and with the rise in extrusion temperature, the microscopic orientation function in the central region increases more than that in the surface region. As the difference in orientation between the outer layer and the central layer is diminished, the boundary between the outer and central layers becomes obscure.

REFERENCES

1. K. Shimamura, J. L. White, and J. F. Feller, *J. Appl. Polym. Sci.*, **26**, 2165 (1981).

2. Y. Ide and Z. Ophir, *Polym. Eng. Sci.*, **23,** 261 (1983).
3. L. C. Sawyer and M. Jaffe, *J. Mater. Sci.*, **21,** 1897 (1986).
4. T. Weng, A. Hiltner, and E. Baer, *J. Mater. Sci.*, **21,** 744 (1986).
5. Y. Takeuchi, Y. Shuto, and F. Yamamoto, *Polymer,* **29,** 605 (1988).
6. E. Baer, A. Hiltner, and T. Weng, *Polym. Mater. Sci. Eng.*, **52,** 88 (1985).
7. M. Kyotani, A. Kaito, and K. Nakayama, *J. Appl. Polym. Sci.*, to appear.
8. T.-S. Chung, *J. Polym. Sci. Polym. Lett. Ed.*, **24,** 299 (1986).
9. K. Itoyama and T. Yamakawa, *Kobunshi Ronbunshu,* **45,** 925 (1988).
10. D. J. Blundell, R. A. Chivers, A. D. Curson, J. C. Love, and W. A. MacDonald, *Polymer,* **29,** 1459 (1988).
11. A. Pirnia and C. S. P. Sung, *Macromolecules,* **21,** 2699 (1988).
12. A. Kaito, M. Kyotani, and K. Nakayama, *Macromolecules,* **24,** 3244 (1991).
13. A. Kaito, M. Kyotani, and K. Nakayama, *Polymer,* **33,** 2672 (1992).
14. G. W. Calundann and M. Jaffe, in *Proceedings of the Robert A. Welch Conference on Chemical Research, XXVI, Synthetic Polymers,* 1982.
15. H. Muramatsu and W. R. Krigbaum, *J. Polym. Sci. Polym. Phys. Ed.*, **24,** 1695 (1986).
16. H. Muramatsu and W. R. Krigbaum, *J. Polym. Sci. Polym. Phys. Ed.*, **25,** 2303 (1986).
17. A. Tealdi, A. Ciferri, and G. Conio, *Polym. Commun.*, **28,** 22 (1987).
18. A. Kaito and K. Nakayama, *Macromolecules,* **25,** 4882 (1992).

Received May 11, 1992
Accepted September 28, 1992